

# Effects of an asymmetrical confined flow on a rectangular cylinder

A. Cigada<sup>a</sup>, S. Malavasi<sup>b</sup>, M. Vanali<sup>a,\*</sup>

<sup>a</sup>*Mechanical Department, Politecnico di Milano, Via La Masa, 34, 20156 Milano, Italy*

<sup>b</sup>*D.I.I.A.R., Politecnico di Milano, Piazza Leonardo da Vinci, 32, 20133 Milano, Italy*

Received 17 December 2004; accepted 17 September 2005

Available online 25 October 2005

---

## Abstract

The effects of an asymmetric confined flow on a cylinder of rectangular cross-section are investigated and discussed. Experiments are performed in a wind tunnel by placing cylinders of different cross-sections at various elevations from the floor of the test-section. The Reynolds number is varied within the range  $6 \times 10^3$ – $4 \times 10^4$ . Forces exciting the cylinder are measured by built-in dynamometers placed inside the cylinder structure. The flow is characterized by mean and fluctuating local velocity components to define the inflow distribution and the ensuing wake region. The mean dimensionless force coefficients are then calculated and analyzed. The frequency analysis of the force components acting on the cylinder provides the dynamic characterization of the loading and of the wake shedding. The experimental results highlight that the presence of the wall strongly influences the system dynamics also when the cylinder is placed at a relatively large elevation from the wall itself. The cylinder aspect ratio governs effects of the wall condition on the force coefficients and the Strouhal number.

© 2005 Elsevier Ltd. All rights reserved.

*Keywords:* Drag; Lift; Cylinders; Strouhal number

---

## 1. Introduction

The fluid-dynamic forces acting on a rectangular cylinder have been mainly investigated for unbounded flow conditions (Okajima, 1982; Blevins, 1984; Naudascher, 1991; Naudascher and Rockwell, 1993; Norberg, 1993; Okajima et al., 1997). The bounding effect of a fixed wall occurs in many applications of civil engineering (e.g., in the case of bridges and/or buildings placed in the proximity of other structures or particular land morphology, both in water or air-flow), and needs to be explored in detail.

Malavasi and Guadagnini (2003) investigated the nature of the fluid-dynamic forces acting on river bridges under flood conditions. They analyzed the influence of the height of the free surface above the obstacle, and found evidence that the bridge height from the bottom of the water channel has an important role in the interpretation of the data.

Here we focus on the effects that the presence of a fixed wall placed at various distances from a rectangular cylinder has on the fluid-dynamic forces acting on the cylinder itself. An experimental campaign was designed and performed in

---

\*Corresponding author. Tel.: +390223998448; fax: +390223998492.

*E-mail addresses:* alfredo.cigada@polimi.it (A. Cigada), stefano.malavasi@polimi.it (S. Malavasi), marcello.vanali@polimi.it (M. Vanali).

a wind tunnel in order to isolate and investigate the effect of the bottom wall. As compared to the work of Malavasi and Guadagnini (2003), we note that the choice to carry out the research in an air stream instead of a water channel is related to the requirement of suppressing any free surface effect. The analysis is performed on a vertical plane, where the wall coincides with the floor of the test chamber, to create the asymmetric condition under investigation.

Despite the simple geometry of the considered model and the wide practical use of cylindrical structures with rectangular cross-section, most research studies on the effect of an asymmetric boundary condition are concerned with structures of circular cross-section (Jarno-Druaux et al., 1995; Lei et al., 1999; Price et al., 2002). The case of a rectangular cylinder placed in unbounded flow can be assumed as a limit case of a bounded flow problem (where the solid surface is placed at an infinite distance from the obstacle). Here, we consider the rectangular cylinder in unbounded flow as a reference condition, to compare against our experimental results. Thus, the range of Reynolds number investigated was set in order to allow an appropriate comparison.

Fluid-dynamic forces on structures can be analyzed in terms of mean and fluctuating components. The latter are important mainly to quantify the response of the structure to turbulent excitation. One can distinguish amongst the following excitation mechanisms involved: (a) extraneously induced excitation (EIE), which is caused by fluctuating velocities or pressures which are independent from any flow instabilities originating from the structure and from the structural motion, with the exception of added-mass effect; (b) instability-induced excitation (IIE), which is caused by an instability of the flow, due to the presence of the structure; (c) movement-induced excitation (MIE), which is due to fluctuating forces arising from movements of the vibrating structure; (d) excitation due to fluid oscillation (EFO), which is caused by a fluid oscillator becoming excited at one of its natural modes. For cases (a), (b) and (c) the exciting forces may or may not be affected by the simultaneous excitation due to fluid oscillation (EFO) (Naudascher, 1991).

The excitation of flow-induced vibrations in a real system is very often a complex physical process, since EIE, IIE, and MIE may occur simultaneously. If, as in our case, one considers a rigidly fastened cylinder of rectangular section and indefinite cross-length (sectional model) in a stationary flow, the type of stresses which are relevant for the phenomenon are EIE and IIE. These depend on both the characteristics of flow and the geometry of the obstacle.

Concerning the IIE excitation mechanism, Deniz and Staubli (1997) proposed the following classification of the wake structure: (a) Leading-Edge Vortex Shedding (LEVS), when flow separation occurs at the cross-section leading edge, with formation of vortices, dominating the near wake of the body (Fig. 1(a)); (b) Impinging Leading-Edge Vortices (ILEV), when a flow separation at the leading edge and impingement of the leading-edge vortices at the side surfaces and/or edges of the body are present (Fig. 1(b)); (c) Trailing-Edge Vortex Shedding (TEVS), when a decisive flow separation at the trailing edge occurs and vortex shedding is analogous to the von Karman street behind circular cylinders (Fig. 1(c)); (d) Alternate-Edge Vortex Shedding (AEVS) when both the leading- and the trailing-edge mechanisms are present (Fig. 1(d)). Depending on the aspect ratio, for a range of incidence angles, the vortex shedding is composed of the alternate separation of one vortex at the leading edge and one at the trailing edge of the structure. This classification is useful for data interpretation since each vortex structure excites the cylinder with a typical frequency component.

The wake structure and the fluid-dynamic loading on the structure under unbounded flow conditions are mainly affected by the following set of parameters: the cylinder aspect ratio ( $l/s$  where  $l$  and  $s$  are the length of the cylinder cross-section parallel and perpendicular to the flow, respectively), the Reynolds number ( $Re$ ), the in-flow turbulence level ( $Tu = v'_{rms}/V$ , where  $v'_{rms}$  and  $V$  are the standard deviation and the mean velocity of the flow in the dominant flow direction), and the incidence angle  $\alpha$ .

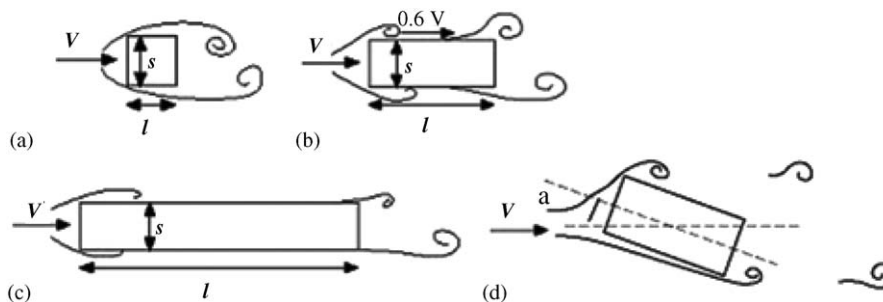


Fig. 1. Mechanism of vortex shedding for IIE source condition on prismatic 2-D obstacle (Deniz and Staubli, 1997).

### 1.1. Influence of the aspect ratio, $l/s$

The aspect ratio is responsible of the type of generated wake and, ultimately, for the structure excitation. This is clearly shown in Figs. 2 and 3, where the drag coefficient and the Strouhal number are, respectively, depicted against the aspect ratio,  $l/s$ .

Specifically, Fig. 2 reveals that the drag coefficient increases with  $l/s$ , for  $0 \leq l/s \leq 0.6$ , increases toward an asymptotic value. The presence of an asymptote is clear if the shear stresses acting on the sides of the body can be considered negligible. The shadowed area in Fig. 2 identifies a range of  $l/s$  affected by a significant data dispersion. This phenomenon is essentially due to the flow turbulence (Simiu and Scanlan, 1996).

With reference to the impact of  $l/s$  on the Strouhal number,  $Sh$ , Fig. 3 shows an abrupt increase of  $Sh$  at  $l/s \approx 3$ . This feature is due to the shift from the LEVS wake typology to TEVS, which occurs together with a significant increase in the vortex shedding frequency and a reduction of the transverse wake size. This behavior was verified by several authors (Deniz and Staubli, 1997; Shimada and Ishihara, 2002). Different experimental conditions highlight a region of unsettled transition, occurring for  $l/s \approx 3$ , in agreement with the type of data dispersion reproduced in Fig. 2 (shadowed area).

### 1.2. Influence of the Reynolds number, $Re$

In the case of a rectangular cylinder, the dependence of the phenomenon on Reynolds number,  $Re$ , was studied by several authors. Norberg (1993) underlines the dependence of the vortex shedding Strouhal number and the drag coefficient upon  $Re$ , for several aspect ratios. The experimental data reported by Norberg ( $70 \leq Re \leq 50\,000$ ;  $0 < l/s \leq 5$ )

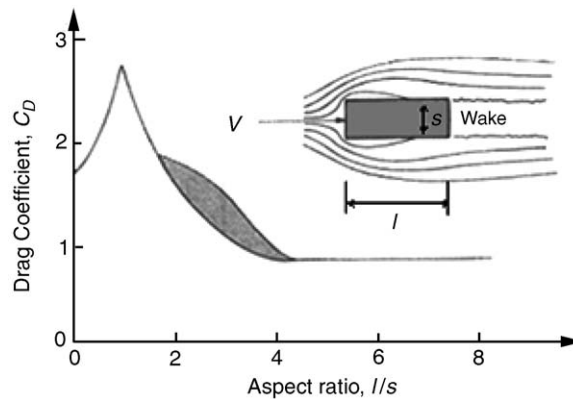


Fig. 2. Drag coefficient versus aspect ratio (Simiu and Scanlan, 1996).

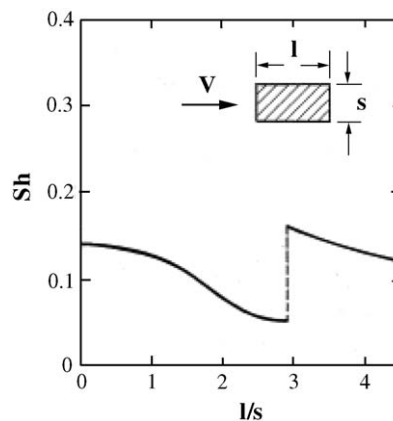


Fig. 3. Strouhal number ( $Sh$ ) of vortex shedding for rectangular cylinder in low-turbulence unbounded cross-flow for Reynolds numbers  $Re \approx 1.0 \times 10^4$  (Naudascher, 1991).

clearly demonstrate that  $Re$  significantly influences the Strouhal number, especially in the range  $2 \leq l/s \leq 3$ , where multiple shedding frequencies are recognizable, but does not visibly influence the values of the drag coefficient. We note that, within the range of values also considered in this work ( $l/s = 3$  and  $Re \geq 7000$ ), the experimental data of Norberg (1993) reveal that both the drag coefficient and the Strouhal number are slightly affected by  $Re$ .

### 1.3. Influence of the in-flow turbulence, $Tu$

The characteristics of the wake are also affected by the in-flow turbulence. Nakamura and Ozono (1987) showed that the main effect of the in-flow turbulence level on the leading sharp edge separation is to shorten the longitudinal size of the separation bubble developing along the lateral side of the obstacle. Naudascher (1991), considering the effects of the interaction between a turbulent flow with rectangular cylinders with aspect ratio  $l/s > 0.6$ , points out that the increase in turbulence level aids the flow reattachment on the side surface of the obstacle and decreases the drag coefficient. Deniz and Staubli (1997) remark that turbulence can strongly influence the location of reattachment as well as the development of the separated shear layers of the ILEV mechanism.

Recently, Noda and Nakayama (2003) studied the effect of turbulence by means of measurements of pressure distribution. The frequency analysis of the pressure components on the cylinder surfaces allowed them to study the dominant frequency of the pressure excitation. In the case of  $l/s = 3$  they noted that the influence of the turbulent in-flow level does not significantly affect the dominant frequency of the phenomenon, and provides a larger contribution to the energy of high-frequency fluctuations.

### 1.4. Influence of the angle of incidence, $\alpha$

The incidence angle,  $\alpha$ , affects significantly the structure of the wake inducing an asymmetrical separation in the flow. The AEVS wake structure, typical of asymmetric conditions, significantly affects the dynamic load on the cylinder when  $\alpha \neq 0$ . This notwithstanding, it is reasonable to expect the influence of  $\alpha$  to be significant for  $\alpha > 2-4^\circ$ , depending on the in-flow turbulence level (Deniz and Staubli, 1997; Hemon and Santi, 2002).

## 2. Experimental set-up

Experiments have been performed in a wind tunnel open-jet test-section of  $0.9 \text{ m} \times 0.9 \text{ m}$  cross-section. At the bottom of the test section a solid wall was placed to crate the asymmetric boundary condition (Fig. 4).

Two different rectangular cylinders have been used: one is characterized by a  $0.04 \text{ m} \times 0.12 \text{ m}$  cross-section and a transversal width of  $0.90 \text{ m}$  (thus producing  $l/s = 3$ , blockage ratio  $\gamma_b = s/h_t = 4.44\%$ , where  $h_t$  is the height of the test section); the second one has the same transversal width and a  $0.04 \text{ m} \times 0.16 \text{ m}$  cross-section (corresponding to  $l/s = 4$ ,  $\gamma_b = 4.44\%$ ).

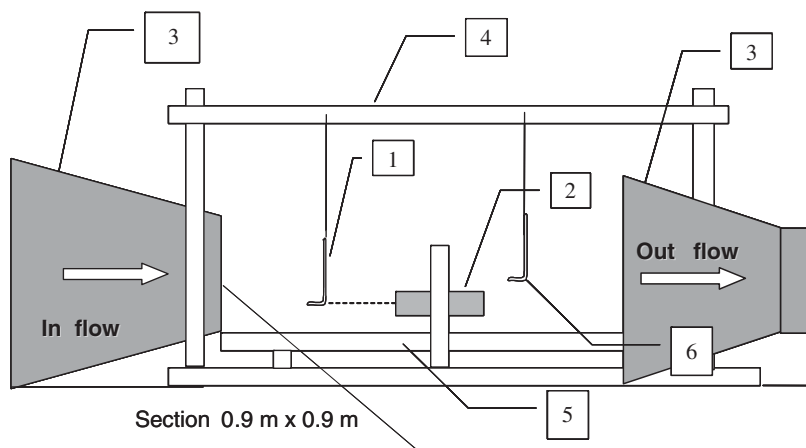


Fig. 4. Experimental set-up: 1. Pitot tube (tube elevation is always corresponding to the cylinder middle section one); 2. rectangular cylinder (model); 3. wind tunnel; 4. iron support; 5. wooden base; 6. hot-wire anemometer.

Two strain-gauge force-sensing elements measure the forces acting on the cylinder. A Pitot tube measures the mean wind speed. A hot-wire anemometer is also employed, in order to perform measurements in the wake of the cylinder.

The two dynamometers were placed inside the cylinder. Their structure has been designed to guarantee the measurement of the anticipated loads (Fig. 2) as well as to cover the frequency range of interest. To limit the influence of the boundary condition at the model sides, the cylinder was subdivided into three parts, and the force induced by the fluid was measured only by the central part. The adoption of two dynamometers allows understanding the wake phenomena upon separately observing the dominant frequencies on the leading edge (L1) and trailing edge (L2) sections (Fig. 5), even if these considerations are possible only in a qualitative sense, e.g. frequency analysis, because the force-sensing elements belong to the same body and act as mechanical coupling between the two load cells.

A detailed description of the dynamometers set-up is provided by Cigada et al. (2001a, b). Force, pressure data (obtained from a strain-gauge differential pressure transducer connected to the Pitot tube) and the output voltage from the hot-wire anemometer conditioning device were acquired via a Spider 8<sup>®</sup> system and a personal computer. The data acquisition system is equipped with a set of built-in anti-aliasing filters. Signals have always been acquired with a sampling frequency of 150 Hz or more. This value has to be compared to the maximum expected vortex shedding frequency, corresponding to 52 Hz at 13 m/s with a Strouhal number  $Sh = 0.16$  (Fig. 3). Special care was devoted to estimating the total uncertainty affecting the measurements. All uncertainties affecting the estimation of each parameter have been calculated, starting from the single transducer uncertainty and then applying the uncertainty propagation law for uncorrelated inputs.

As an example, Fig. 6 depicts the uncertainty on the estimation of the force coefficients for different Reynolds numbers. It can be seen that uncertainty is large at the lowest Reynolds number. This is mainly due to the small

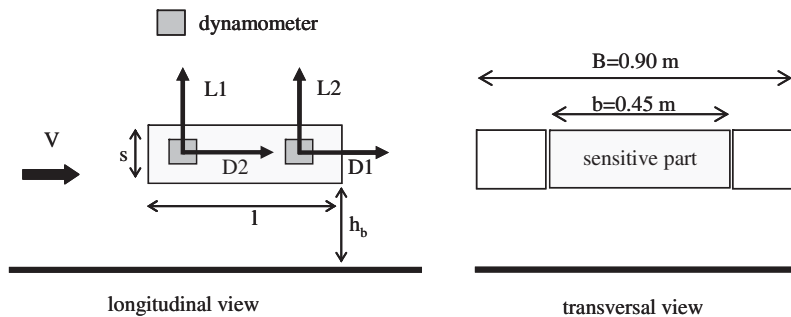


Fig. 5. Dynamometers inside the cylinder.

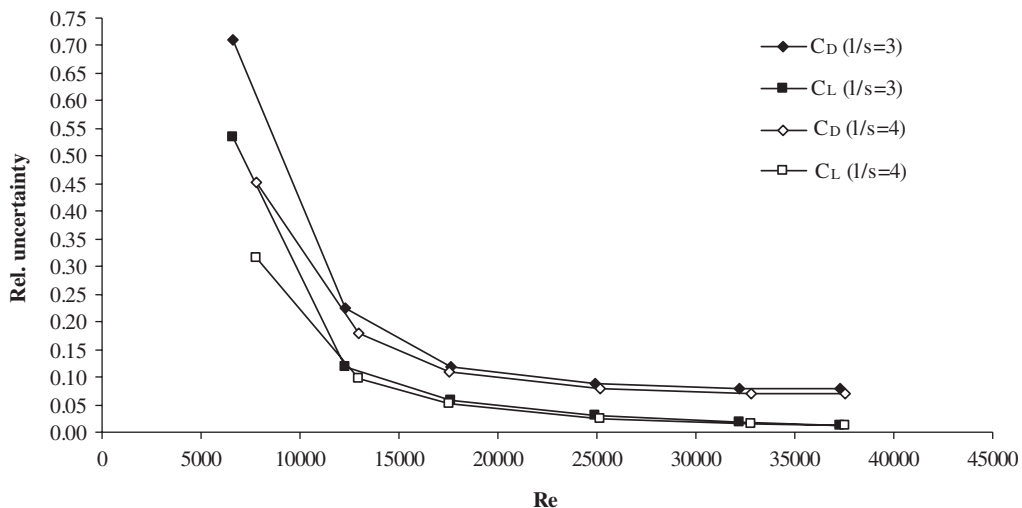


Fig. 6. Relative uncertainty affecting force coefficients.

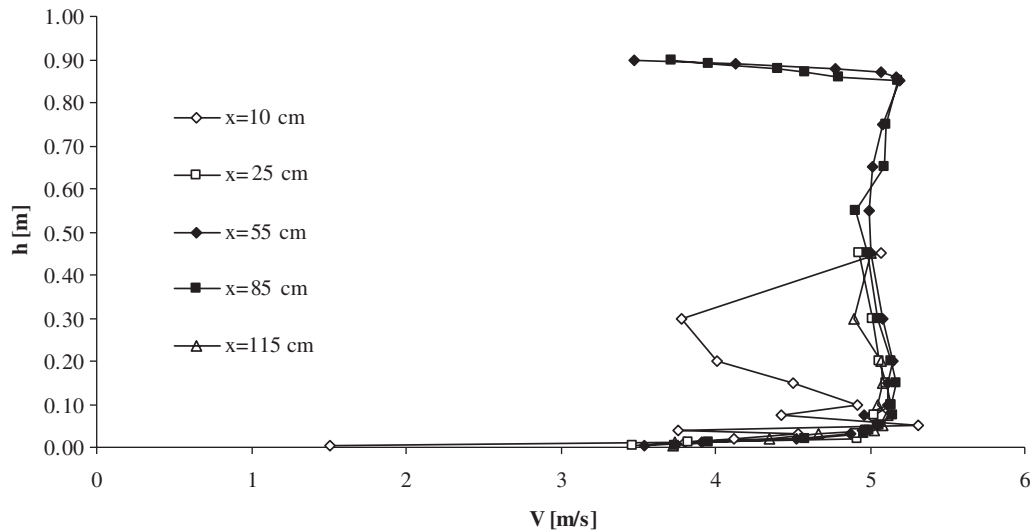


Fig. 7. Wind speed profiles in the chamber (the origin on the  $x$  coordinate corresponds to the inlet section of the wind tunnel).

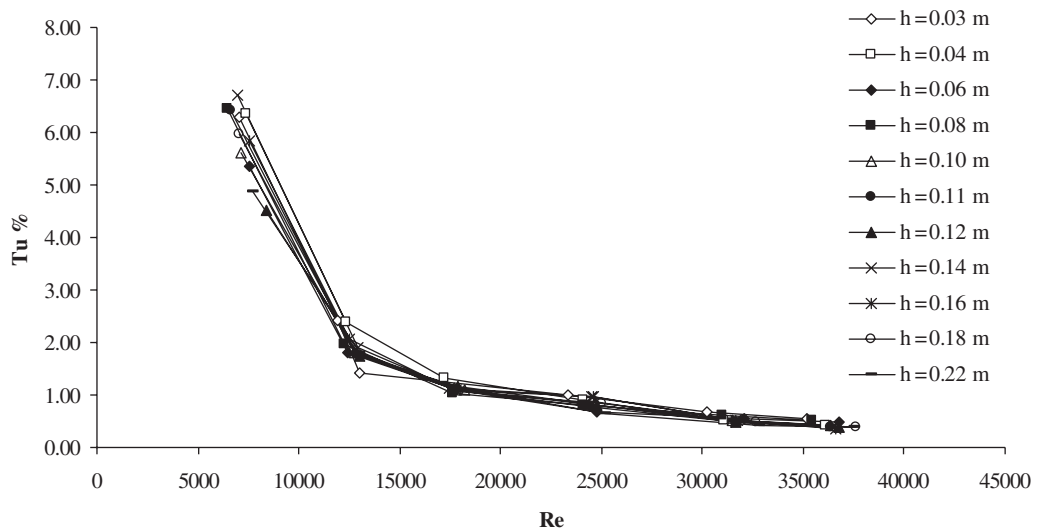


Fig. 8. Dependence of turbulence level,  $Tu$ , on Reynolds number,  $Re$ , and elevations,  $h$ , from the bottom wall.

difference between the pressure values measured at the Pitot tube. The uncertainty on velocity measurements also affects the reconstruction of the wind speed profiles measured across the test-section.

During the tests, each cylinder with the dynamometers was placed at a distance of 90 cm from the entrance of the open test section and at different elevations, ranging from  $h_b/s = 0.15$  to 5. Measurements were then taken for  $6 \times 10^3 < Re < 4 \times 10^4$ . Data were sampled for at least 5 min to ensure the stability of the proper statistics of the estimates.

The aerodynamic force coefficients have then been calculated for all the tested conditions.

All test conditions were monitored to provide meaningful comparisons with the significant references. As an example, Fig. 7 depicts profiles of wind speed at the test section in the absence of the obstacle, at a nominal wind speed of 5 m/s. Velocity profiles have been measured at various verticals across the open test section. Measurements have been taken at vertical elevations varying from 1 to about 90 cm from the bottom. The velocity is constant at elevations larger than 4 cm as the boundary layer is fully developed. As expected, the profile reconstructed in the proximity of the inlet section of the wind tunnel is highly irregular. These measurements allowed assessing the boundary layer height.

The turbulence level ( $Tu$ ) has been calculated for all tests and the results are presented in Fig. 8.

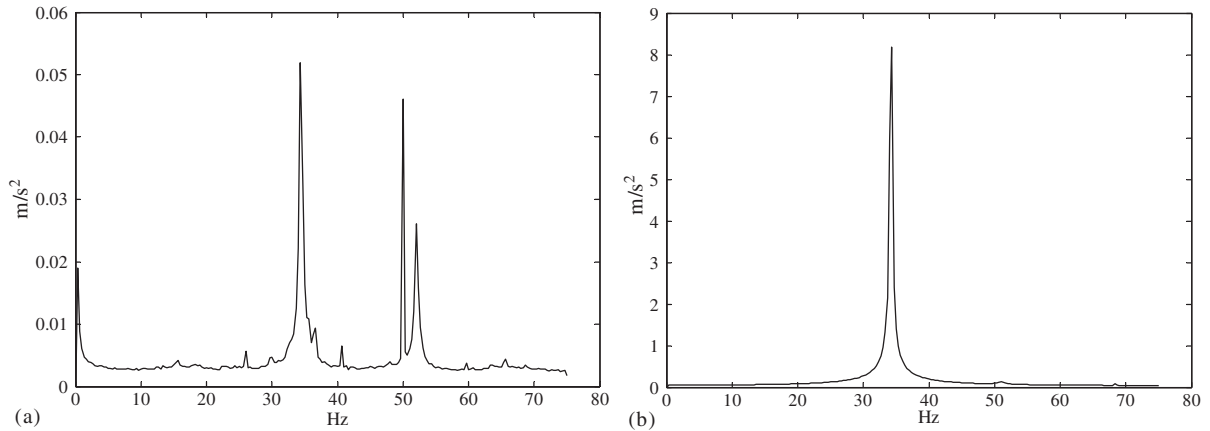


Fig. 9. Frequency spectrum of the acceleration measured on the rectangular cylinder with  $l/s = 3$ . (a) Frequency spectrum of the accelerometer,  $Re = 1.33 \times 10^4$ ; (b) frequency spectrum of the accelerometer,  $Re = 2.65 \times 10^4$ .

Table 1  
Natural frequency of the cylinders on lift direction

| Aspect ratio $l/s$ | Natural frequency in lift direction $f_{oL}$ (Hz) |
|--------------------|---|
| 3                  | 34.5  |
| 4                  | 33.0  |

The stiffness of the cylinder was then analyzed to verify that movements of the cylinder (which might arise and might be important in case of dynamic amplification) did not affect frequencies typical of the vortex shedding phenomena in the range of the tested velocities. The tests were performed by placing an accelerometer on the top of the cylinder and varying the velocity of the flow field. Fig. 9 depicts the spectra of two experimental accelerations frequency, for different wind speeds. Fig. 9(a) allows recognizing three distinct peaks in the spectrum. The first peak is displayed at 50 Hz, and is related to electrical noise (it has been filtered out for analysis purposes). Two additional peaks are displayed at 34.5 and 52.5 Hz. These are related to the first two natural frequencies of the cylinder mounted on the dynamometers, which always exhibit some elastic behavior even if designed to reduce it. Fig. 9(b) reveals that the cylinder is excited at its first natural frequency for a wind speed of 10 m/s, thus leading to much larger acceleration amplitudes. These data have been collected during the pre-testing phase and Table 1 reports the natural frequency of the cylinder along the lift direction for the two tested models. These frequencies are close to those of the vortex shedding of the rectangular cylinders tested for a wind velocity of about 10 m/s, as can be verified by the Strouhal number of a rectangular cylinder in an unbounded flow (Fig. 3).

Dynamic measurements in a range close to 10 m/s were discarded and special care was put on the analysis of measurements in the speed range 7–13 m/s, where the vortex shedding frequencies are close to the first vertical natural frequency of the structure.

### 3. Results

The main results of the analysis are here presented and discussed. We start by recalling the definition of the drag coefficient,

$$C_D = \frac{2(D1 + D2)}{\rho V^2 bs} \quad (1)$$

and the lift coefficient,

$$C_L = \frac{2(L1 + L2)}{\rho V^2 bs}, \quad (2)$$

where  $D_1$ ,  $D_2$ ,  $L_1$  and  $L_2$  are the drag and the lift components of the loading on the cylinder (Fig. 5),  $\rho$  is the air density and  $b$  is the transversal dimension of the sensing portion of the cylinder (Fig. 5).

We have measured: (i) the force coefficients ( $C_D$ ,  $C_L$ ) on cylinders with two different aspect ratios ( $l/s = 3, 4$ ), placed at several distances from a solid boundary surface and for various Reynolds numbers ( $Re$ ); (ii) the Strouhal number ( $Sh$ ) for the same geometry and flow conditions. The dominant wake frequencies are derived from the frequency analysis of the forces acting on the cylinder and the velocity in the wake region (the sign convention is shown in Fig. 5).

### 3.1. Force coefficients

Figs. 10 and 11 show the dependence of the experimental  $C_D$  on the dimensionless distance ( $h_b/s$ ), for  $6 \times 10^3 < Re < 4 \times 10^4$ , and aspect ratio  $l/s = 3$  and 4, respectively.

First, we note the different degree of scattering of the measurements as a function of  $Re$ . For the lowest  $Re$ , this is related to the large uncertainty affecting the low velocity measurements ( $Re \approx 7 \times 10^3$ ), as shown in Fig. 6. The reduction of the measurement scatter at larger  $Re$  is in agreement with the findings of Simiu and Scanlan (1996), who analyzed unbounded flow conditions and ascribed the observed scatter to the increase of the flow turbulence in the wake region. Data from Fig. 8 clearly show a reduction of turbulence with increasing  $Re$ .

For both aspect ratios,  $C_D$  is not significantly influenced by the presence of the bottom floor when  $h_b/s > 3$ . In this range of  $h_b/s$  our experimental values of  $C_D$  agree with those of Simiu and Scanlan (1996).

In contrast, a significant influence of the bottom wall is evidenced in the region  $h_b/s < 3$ . Reducing the distance between the cylinder and the wall does not significantly affect the general (qualitative) behavior of the system for the two aspect ratios tested ( $l/s = 3$  and 4). For  $l/s = 3$  (Fig. 10), we note a slight increase of  $C_D$  in the range  $3 \leq h_b/s \leq 1.5$ ; it then sharply decreases to a  $C_D$  value of 0.7 when the cylinder is very close to the bottom wall ( $h_b/s = 0.25$ ). For  $l/s = 4$  (Fig. 11), the increase in the  $C_D$  value for  $3 \leq h_b/s \leq 1.5$  is less significant, and the fall out for decreasing values of  $h_b/s$  leads to the same  $C_D$  of about 0.7 for  $h_b/s = 0.25$ . We also note that  $Re$  does not significantly affect the  $C_D$  coefficient within the tested range, similarly to what reported for the unbounded flow condition (Okajima, 1982; Naudascher, 1991; Norberg, 1993).

The dependence of  $C_L$  on  $h_b/s$  and  $Re$  is shown in Figs. 12 and 13 for the two tested models. The trend displayed by  $C_L$  highlights the influence of the bottom wall for  $h_b/s < 3$ , which is more pronounced than that noted for  $C_D$ .

As opposed to  $C_D$ , the behavior of  $C_L$  changes significantly with  $l/s$ . Fig. 12 ( $l/s = 3$ ) shows a significant reduction of  $C_L$  for  $h_b/s < 3$ , which attains negative values for  $2.5 \leq h_b/s \leq 0.7$ . The trend changes for  $h_b/s < 1$  and  $C_L$  becomes positive, reaching values of  $C_L \approx 1.15$  for  $h_b/s = 0.2$ . In the case of  $l/s = 4$  (Fig. 13) we note the absence of significant negative  $C_L$  values. For  $h_b/s < 2.5$ , after an instability range ( $1.5 < h_b/s < 2.5$ ) where the lift coefficient shifts between positive and negative low values,  $C_L$  increases rapidly with the reduction of  $h_b/s$ , to reach positive values ( $C_L = 1.6 \div 1.9$ ), which are considerably larger than those observed for  $l/s = 3$ . A clear reduction of the lift coefficient with the increase of the Reynolds number is noted for low values of  $h_b/s$ .

The lift coefficient is significantly affected by the presence of the bottom wall. It is different from zero in the range  $0 < h_b/s \leq 3$  for  $l/s = 3$  and  $0 < h_b/s \leq 2.5$  for  $l/s = 4$ .

The analysis of the pitch on the structure does not give additional information as the trend of pitch coefficient with  $h_b/s$  is similar to that found for the lift coefficient  $C_L$ .

### 3.2. Shedding frequencies

The effects of the asymmetrical flow condition on the cylinder are also studied by means of frequency analysis of the lift component. Since the values of the first resonant frequencies are  $f_{0L} = 34.5$  Hz for  $l/s = 3$  and  $f_{0L} = 33$  Hz for  $l/s = 4$ , the force frequency analysis was provided only for  $Re < 2 \times 10^4$  (which is the range where the dominant frequencies of the phenomenon are far away from the resonant frequencies).

We start by analyzing the cases with  $h_b/s = 5$ , to compare our results with those obtained under unbounded flow conditions and provided in literature. The frequency spectra of the force measurements taken at a  $Re = 1.33 \times 10^4$  for both aspect ratios here considered are depicted in Fig. 14. The two lift components given by each load cell are depicted separately. Only one dominant frequency is recognizable for the downstream lift channel (L2) for  $l/s = 4$  (Fig. 14(a)), thus leading to a Strouhal number estimation of about 0.12. Fig. 14(b) reveals two dominant frequencies, one for each of the considered lift channel. The frequency found on the upstream lift channel (L1) leads to a Strouhal number of about 0.04, while the dominant frequency of channel (L2) renders an estimate of the Strouhal number of 0.13. Our results are compared with those available in the literature in Fig. 15, showing a good agreement.



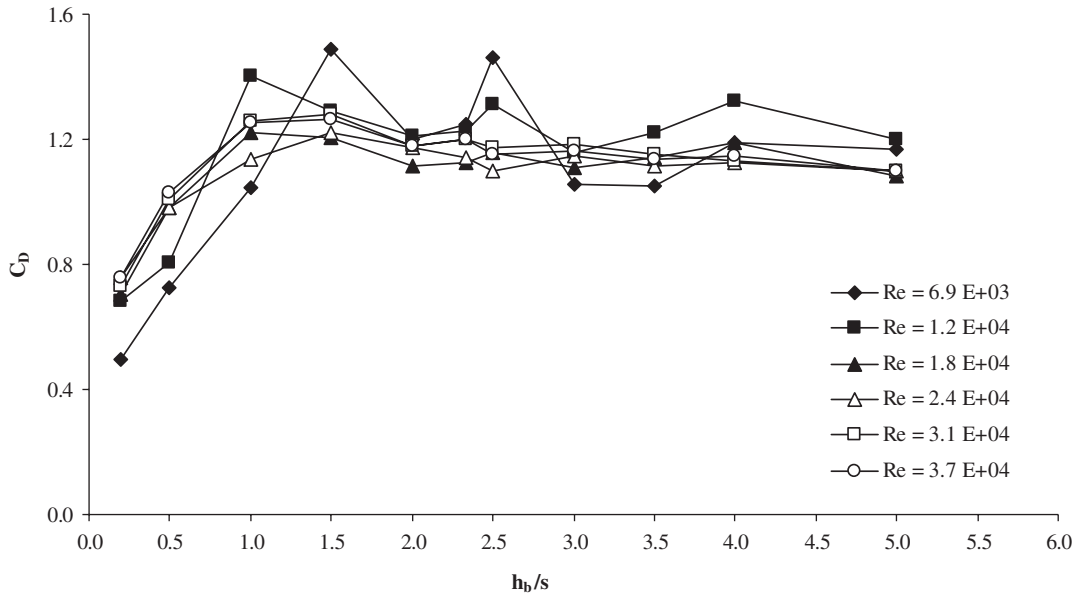


Fig. 10. Dependence of  $C_D$  on  $h_b/s$  and  $Re$  for  $l/s = 3$ .

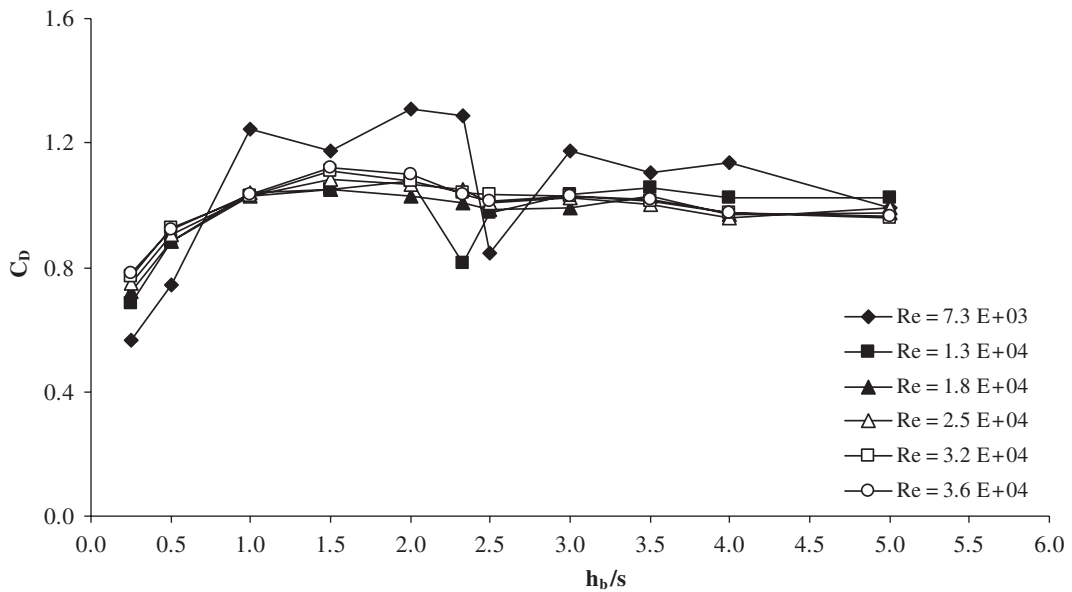


Fig. 11. Dependence of  $C_D$  on  $h_b/s$  and  $Re$  for  $l/s = 4$ .

Our results evidence the presence of both frequencies on the lift signal; these correspond to the jump in the Strouhal number and are identified by other authors. This jump is caused by a change in the vortex shedding mechanism. Use of a twin dynamometer installed inside the cylinder allowed to investigate the difference between the LEVS frequency content and TEVS shedding frequencies. Since we used a rigid cylinder, no reliable assumption on the force distribution could be provided.

Fig. 14 reveals that the characteristic frequency of the TEVS mechanism dominates the vortex shedding phenomenon and it acts mainly on the downstream lift channel (L2) for  $l/s = 4$ . On the contrary, for  $l/s = 3$  the LEVS mechanism, characterized by the lowest frequency, is significant. It is mainly present on the upstream lift channel (L1), while on the

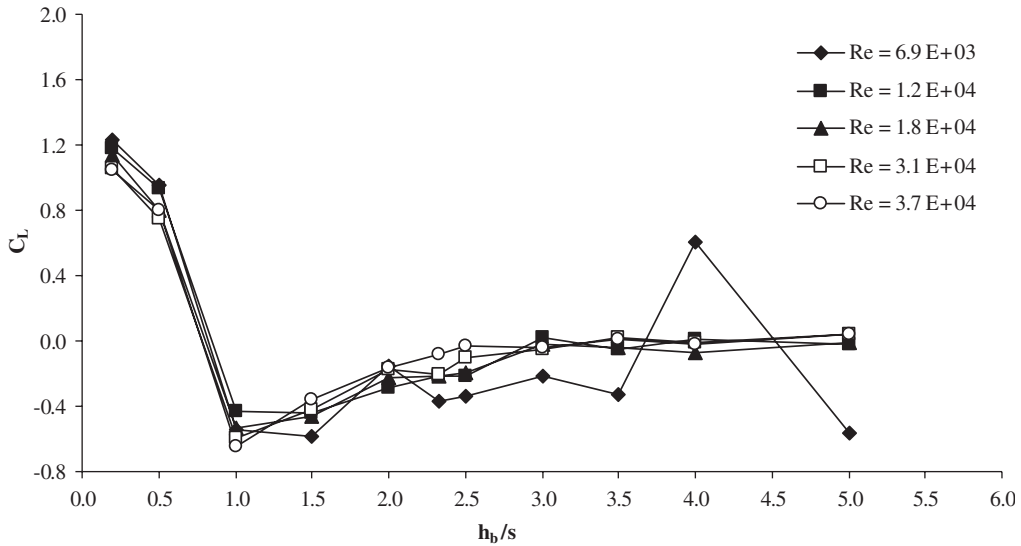


Fig. 12. Dependence of  $C_L$  on  $h_b/s$  and  $Re$  for  $l/s = 3$ .

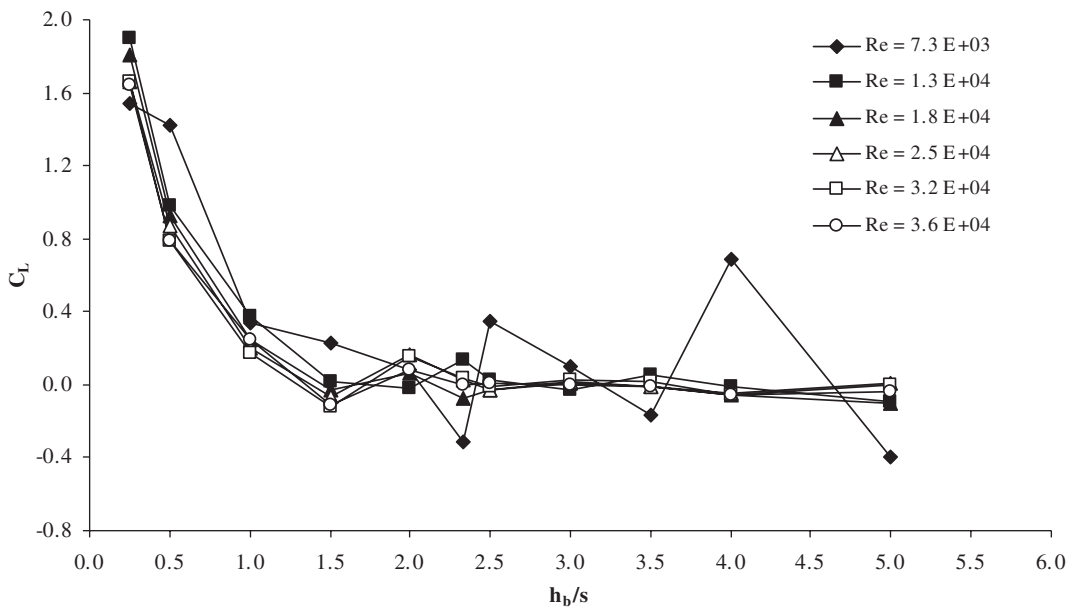


Fig. 13. Dependence of  $C_L$  on  $h_b/s$  and  $Re$  for  $l/s = 4$ .

downstream lift channel (L2) the frequency of the TEVS mechanism conserves the main peak. These results suggest that, while for  $l/s = 4$  the influence of the LEVS on the vortex shedding is negligible, it becomes significant for  $l/s = 3$ .

In order to confirm the results and to explain the presence of the peak at the frequency of about 0.5 Hz, which is recognizable on both the lift components and the two aspect ratios, the frequency spectrum of the flow speed in the wake and the wind tunnel structure vibration are investigated jointly by means of a hot wire probe and an accelerometer.

Fig. 16, which shows the frequency spectrum of the flow speed with in the wake, highlights the same dominant frequencies recognizable in Fig. 14(b); acceleration measurements confirmed that the lowest frequency peak evidenced in the frequency analysis of force and velocity is due to the movement of the wind tunnel, pressure-induced deflections.

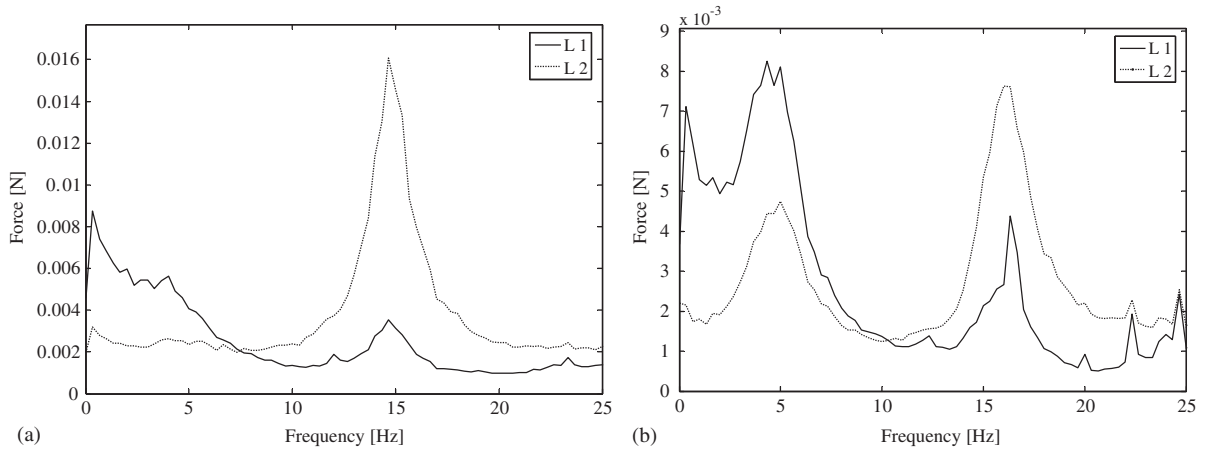


Fig. 14. Frequency spectrum of the lift components for  $h_b/s = 5$  and  $Re = 1.33 \times 10^4$ : (a)  $l/s = 4$ ; (b)  $l/s = 3$ .

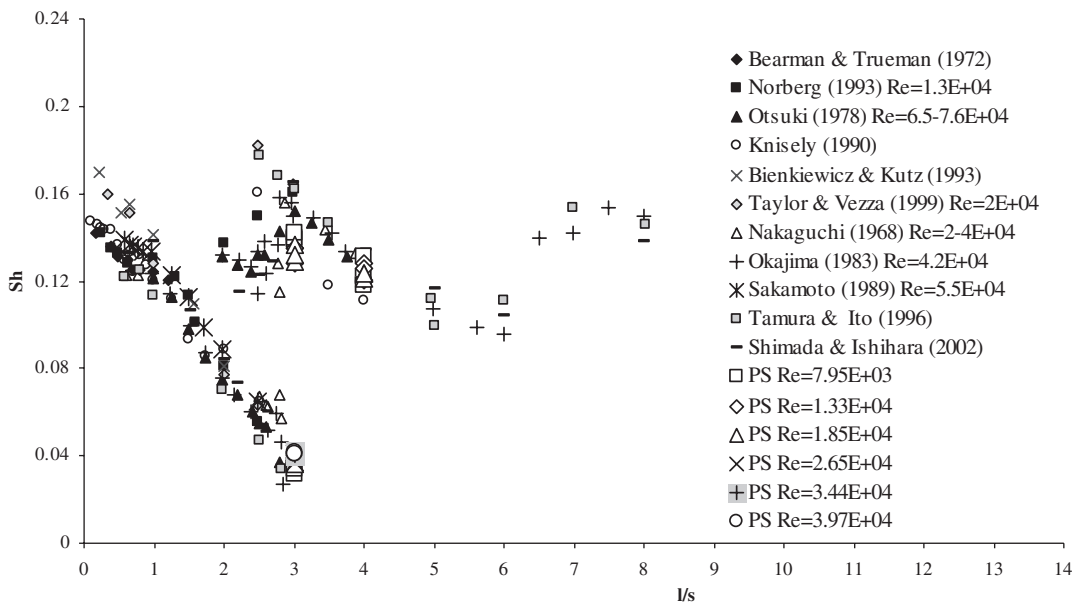


Fig. 15. Strohual number versus  $l/s$ ; data collected in Shimada and Ishihara (2002) and the present study.

It is interesting to study the influence of the boundary wall on the dynamic components of the forces. Fig. 17 shows the force frequency spectrum of the lift channel (L2) measured at  $Re = 1.33 \times 10^4$  and  $l/s = 4$  for different  $h_b/s$ . It can be noted that the effect of the wall slightly increases the vortex shedding frequency at the trailing edge (TEVS). This is probably due to an increase in the local speed and to the presence of the boundary, which limits the vortex development while the magnitude of the peak decreases as the model approaches the solid wall. The case of  $l/s = 3$  is depicted in Figs. 18 and 19, where the downwind (L2) and the upwind (L1) forces are analyzed. While two dominant frequencies are recognizable here, the effect of the proximity of the solid wall does not change; when the cylinder elevation decreases, the dominant frequencies change and it can be noted the magnitude of the peak decreases (Figs. 18 and 19). It is nevertheless interesting to note that, with  $l/s = 3$ , the peak decreases faster for the leading edge than for the trailing edge vortex, for both lift channels (L1, L2). This result might be explained as follows: the leading edge vortex developing on the front side of the cylinder is much more limited by the presence of the solid wall than the trailing edge vortex, which detaches from the rear face of cylinder. The peak arising around 24 Hz for the lowest  $h_b/s$  has been

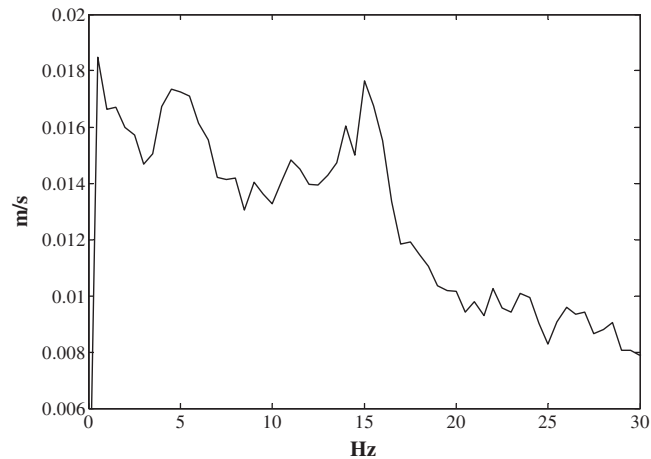


Fig. 16. Frequency of the flow speed in the wake  $Re = 1.33 \times 10^4$ ,  $h_b/s = 5$ , spectral resolution 0.3 Hz, sampling frequency 150 Hz.

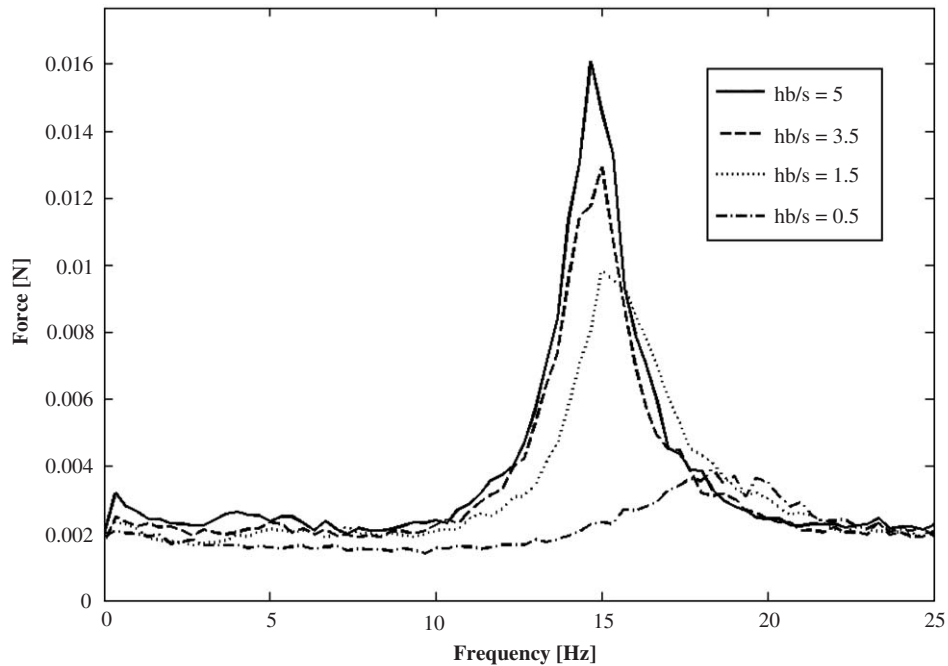


Fig. 17. Frequency spectrum of the lift channel (L2) for  $Re = 1.33 \times 10^4$ ,  $l/s = 4$  at different  $h_b/s$ , spectral resolution 0.3 Hz, sampling frequency 150 Hz.

identified as a resonant frequency of the structure supporting the cylinder, which may or may not be excited, depending on the cylinder position, due to the fact that we operate in an open chamber test section.

In order to resume the influence of the boundary condition on the Strohal number for both  $l/s = 3$  and 4 in Fig. 20 and Fig. 21, respectively, the values of  $Sh$  versus  $h_b/s$  is shown for all Reynolds numbers considered. Two dominant frequencies are present in the case of  $l/s = 3$ , and both these frequencies and the one relative to case  $l/s = 4$  increase as the cylinder is moved towards the wall ( $h_b/s$  decreases). For the lowest  $h_b/s$  values it is difficult to evidence a dominant frequency in the spectrum, leading to a higher dispersion in the result; in certain cases no result is given as it was impossible to identify the most important peak.

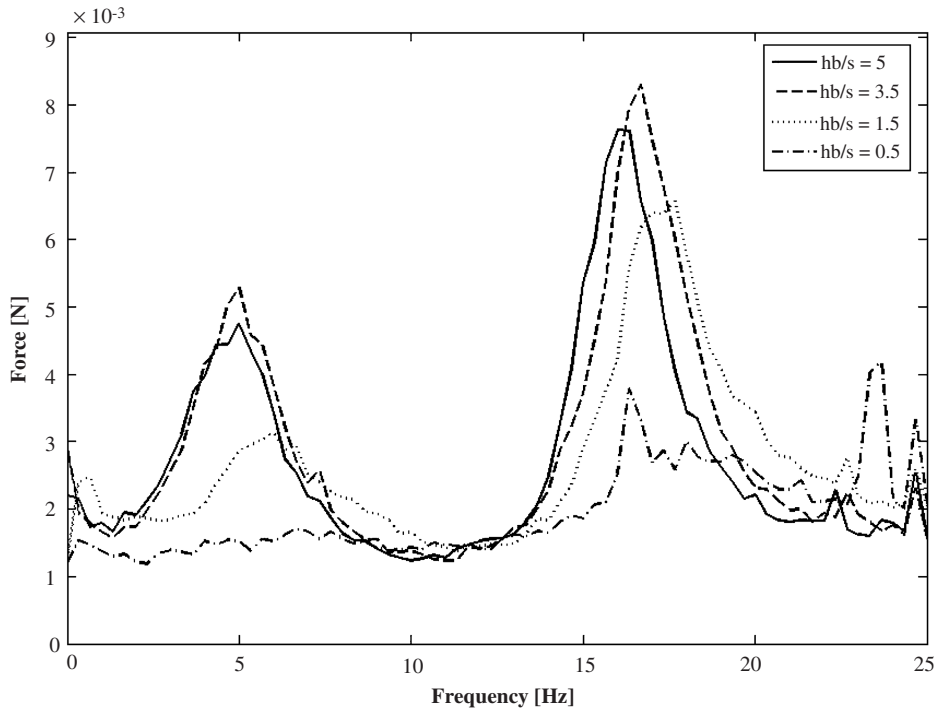


Fig. 18. Frequency spectrum of the lift channel (L2) for  $Re = 1.33 \times 10^4$ ,  $l/s = 3$  at different  $h_b/s$ , spectral resolution 0.3 Hz, sampling frequency 150 Hz.

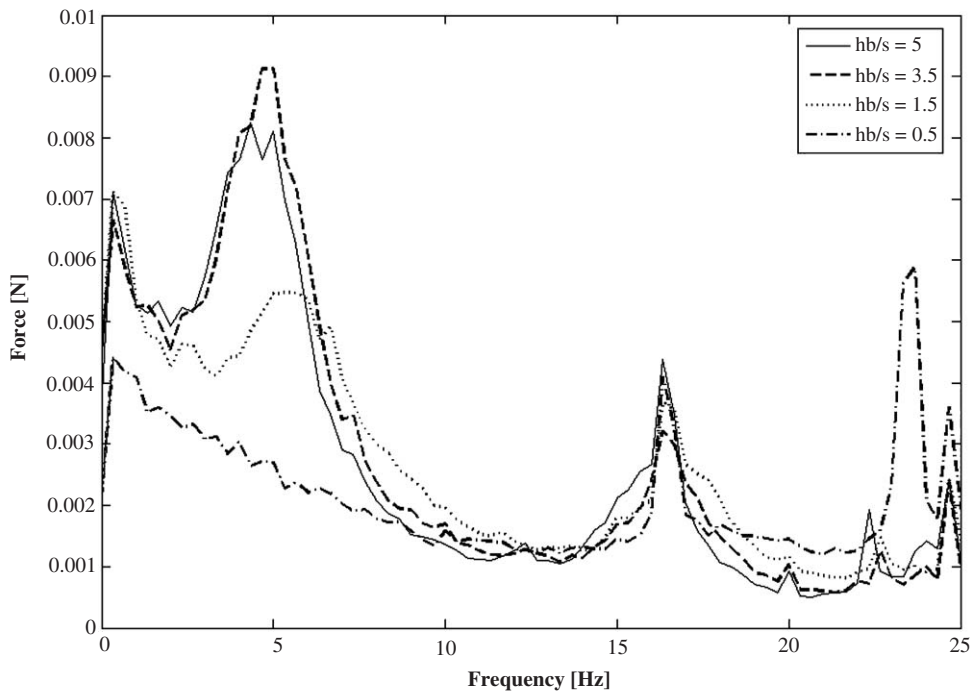


Fig. 19. Frequency spectrum of the lift channel (L1) for  $Re = 1.33 \times 10^4$ ,  $l/s = 3$  at different  $h_b/s$ , spectral resolution 0.3 Hz, sampling frequency 150 Hz.

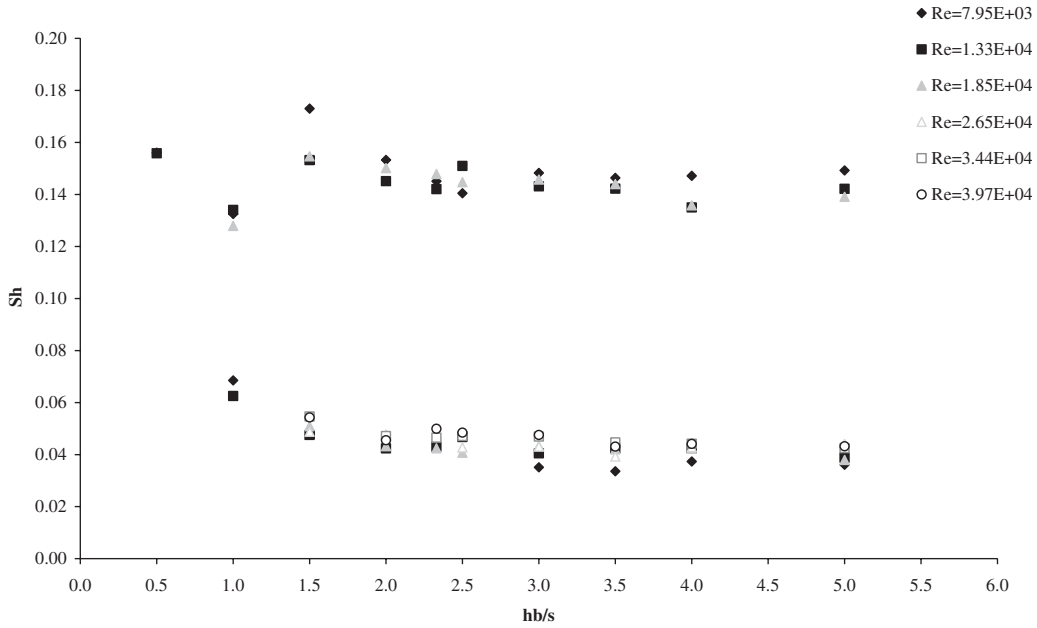


Fig. 20. Strouhal number versus  $h_b/s$ ,  $l/s = 3$  at different Reynolds numbers.

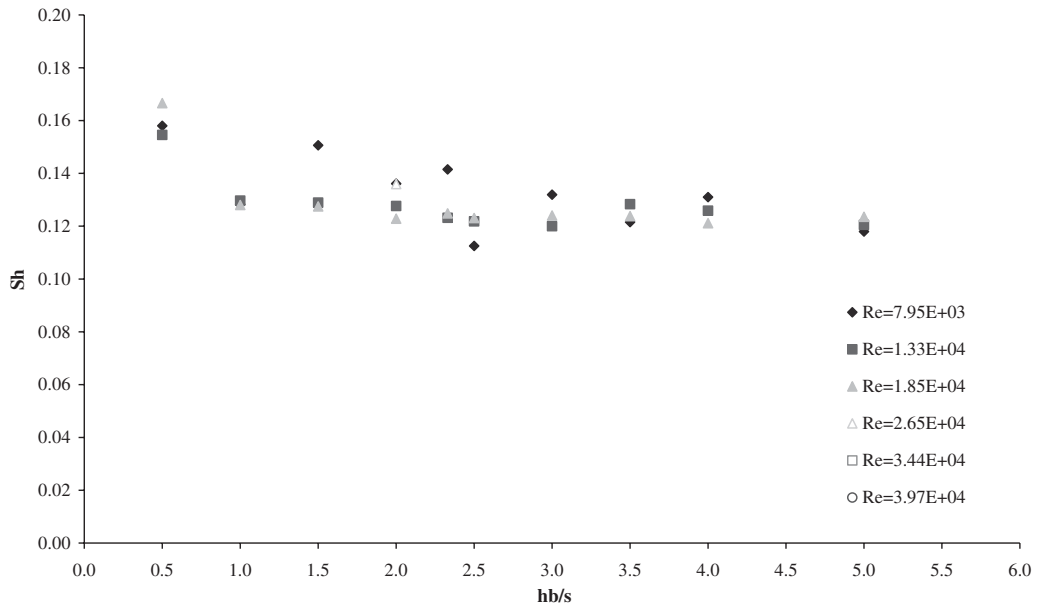


Fig. 21. Strouhal number versus  $h_b/s$ ,  $l/s = 4$  at different Reynolds numbers.

#### 4. Conclusions

Our work leads to the following major conclusions:

- (i) A system of twin dynamometers placed inside the cylinder allowed for a better understanding of the vortex shedding phenomenon. It allowed a qualitative separation of the leading and trailing-edge vortex shedding mechanisms. Our data for quasi-unbounded flow conditions ( $h_b/s > 4$ ) agree with those reported in the literature.

- (ii) The force coefficients, derived by force measurements, were influenced by the bottom wall up to an elevation of  $h_b/s \approx 2.5$  for  $l/s = 4$  and of  $h_b/s \approx 3.0$  for  $l/s = 3$ . These values could be considered unaffected by the Reynolds number in the range considered. The drag coefficient displays almost the same behavior for both aspect ratios (Figs. 10 and 11). On the other hand, the lift coefficient is significantly affected by  $l/s$ . For  $l/s = 3$  when  $h_b/s$  decreases  $C_L$  first goes down to negative values, then, after  $h_b/s = 1$ ,  $C_L$  rapidly switches to positive values (Fig. 12).  $C_L$  displays a monotonic behavior for  $l/s = 4$  and it increases when the elevation of the cylinder from the bottom floor decreases (Fig. 13).
- (iii) The frequency analysis of the force components shows the negligible influence of the wall surface when the wall is placed at an elevation  $h_b/s > 4$ . In this case, our data are in good agreement with those obtained by several authors for unbounded flow conditions (Fig. 15). When the elevation of the cylinder decreases, the frequency analysis of the two lift components (L1 and L2) for  $l/s = 3$  shows that the magnitude of the force related to the leading edge vortex shedding frequency decrease faster than that related to the trailing edge frequency. The dominant frequency value slightly increases when the distance between the cylinder and the floor decreases (Figs. 18 and 19). On the other hand, the increase of the vortex shedding frequency is more evident for  $l/s = 4$ , where only the frequency of the trailing vortex is present. As the height of the cylinder above the floor is reduced, a monotonic reduction of the peak amplitude and an increase in the frequency of the vortex can be observed (Fig. 17).

The same results have been found for all Reynolds numbers as summarized in Figs. 20 and 21 for the two aspect ratios considered.

## References

- Blevins, R.D., 1984. Applied Fluid Dynamics Handbook. Van Nostrand Reinhold Company, New York.
- Cigada, A., Falco, M., Zasso, A., 2001a. Development of new systems to measure the aerodynamic forces on section models in wind tunnel testing. *Journal of Wind Engineering and Industrial Aerodynamics* 89, 725–746.
- Cigada, A., Malavasi, S., Vanali, M., 2001b. Direct forces measurement on a submerged bridge model. In: First International Conference on Fluid Structure Interaction, 26–28 September, Halkidiki, Greece.
- Deniz, S., Staubli, Th., 1997. Oscillating rectangular and octagonal profiles: integration of leading- and trailing-edge vortex formation. *Journal of Fluids and Structures* 11, 3–31.
- Hemon, P., Santi, F., 2002. On the aeroelastic behavior of rectangular cylinder in cross-flow. *Journal of Fluids and Structures* 16, 855–889.
- Jarno-Druaux, A., Sakout, A., Lambert, E., 1995. Interference between a circular cylinder and a plane wall under waves. *Journal of Fluids and Structures* 9, 215–230.
- Lei, C., Cheng, L., Kavanagh, K., 1999. Re-examination of the effect of a plane boundary on force and vortex shedding of a circular cylinder. *Journal of Wind Engineering and Industrial Aerodynamics* 80, 263–286.
- Malavasi, S., Guadagnini, A., 2003. Hydrodynamic load on river bridge. *ASCE Journal of Hydraulic Engineering* 129, 854–861.
- Nakamura, Y., Ozono, S., 1987. The effect of turbulence on a separated and reattaching flow. *Journal of Fluid Mechanics* 178, 477–490.
- Naudascher, E., 1991. IAHR Design Manual: Hydrodynamic Forces. A.A. Balkema Publishers, Rotterdam.
- Naudascher, E., Rockwell, D., 1993. IAHR Design Manual: Flow Induced Vibrations—An Engineering Guide. A.A. Balkema Publishers, Rotterdam.
- Noda, H., Nakayama, A., 2003. Free-stream turbulence effects on instantaneous pressure and forces on cylinder of rectangular cross section. *Experiments in Fluids* 34, 332–344.
- Norberg, C., 1993. Flow around rectangular cylinders, pressure forces and wake frequencies. *Journal of Wind Engineering and Industrial Aerodynamics* 49, 187–196.
- Okajima, A., 1982. Strouhal number of rectangular cylinder. *Journal of Fluid Mechanics* 123, 379–398.
- Okajima, A., Yi, D., Kimura, S., Kiwata, T., 1997. The blockage effects for an oscillating rectangular cylinder at moderate Reynolds number. *Journal of Wind Engineering and Industrial Aerodynamics* 69–71, 997–1011.
- Price, S.J., Sumner, D., Shmith, J.G., Leong, K., Paidoussis, M.P., 2002. Flow visualization around a circular cylinder near to a plane wall. *Journal of Fluids and Structures* 16, 175–191.
- Shimada, K., Ishihara, T., 2002. Application of modified  $k-\epsilon$  model to the prediction of aerodynamic characteristics of rectangular cross section cylinders. *Journal of Fluids and Structures* 16, 465–485.
- Simiu, E., Scanlan, R.H., 1996. Wind Effects on Structures. Wiley, New York.